Available online at www.sciencedirect.com
ScienceDirect
Biochimica et Biophysica Acta 1774 (2007) 1192 – 1198
Biochimica et Biophysica Acta
BBA
www.elsevier.com/locate/bbapap

Variation in relative substrate specificity of bifunctional β-D-xylosidase/α-L-arabinofuranosidase by single-site mutations: Roles of substrate distortion and recognition

Douglas B. Jordan *, Xin-Liang Li

Fermentation Biotechnology Research Unit, National Center for Agricultural Utilization Research, U.S. Department of Agriculture, Agricultural Research Service, 1815 N. University Street, Peoria, IL 61604, USA

Received 25 April 2007; received in revised form 5 June 2007; accepted 25 June 2007
Available online 6 July 2007

Abstract

To probe differential control of substrate specificities for 4-nitrophenyl-α-L-arabinofuranoside (4NPA) and 4-nitrophenyl-β-D-xylopyranoside (4NPX), residues of the glycone binding pocket of GH43 β-D-xylosidase/α-L-arabinofuranosidase from *Selenomonas ruminantium* were individually mutated to alanine. Although their individual substrate specificities $(k_{cat}/K_m)^{4NPX}$ and $(k_{cat}/K_m)^{4NPA}$ are lowered 330 to 280,000 fold, D14A, D127A, W73A, E186A, and H248A mutations maintain similar relative substrate specificities as wild-type enzyme. Relative substrate specificities $(k_{cat}/K_m)^{4NPX}/(k_{cat}/K_m)^{4NPA}$ are lowered by R290A, F31A, and F508A mutations to 0.134, 0.407, and 4.51, respectively, from the wild type value of 12.3 with losses in $(k_{cat}/K_m)^{4NPX}$ and $(k_{cat}/K_m)^{4NPA}$ of 18 to 163000 fold. R290 and F31 reside above and below the C4 OH group of 4NPX and the C5 OH group of 4NPA, where they can serve as anchors for the two glycone moieties when their ring systems are distorted to transition-state geometries by raising the position of C1. Thus, whereas R290 and F31 provide catalytic power for hydrolysis of both substrates, the native residues are more important for 4NPX than 4NPA as the xylopyranose ring must undergo greater distortion than the arabinofuranose ring. F508 borders C4 and C5 of the two glycone moieties and can serve as a hydrophobic platform having more favorable interactions with xylose than arabinofuranose.
Published by Elsevier B.V.

Keywords: Glycoside hydrolase; GH43; Stereoelectronic effect; Near attack conformation; Transition state

1. Introduction

Bifunctional enzymes displaying β-D-xylosidase (EC 3.2.1.37) and α-L-arabinofuranosidase (EC 3.2.1.55) activities are found among diverse biological species, glycoside hydrolase (GH) families (GH3, GH43, GH51, and GH54; based on protein sequence), and glycoside hydrolase clans (GH-A, GH-F and unassigned clan; based on three-dimensional structures and protein sequence relationships) in the CAZy database (Carbohydrate Active Enzymes database, http://www.cazy.org/) [1–3]. Furthermore, β-D-xylosidase/α-L-arabinofuranosidase (XA) enzymes are known to catalyze hydrolysis of glycoside bonds through either of two distinct, classical mechanisms: single displacement with inversion of anomeric stereochemistry or double displacement with retention of anomeric stereochemistry [4–11]. The common link of bifunctionality, which is not shared uniformly among XA enzymes as some have greater xylosidase activity (determined with substrate 4NPX, 4-nitrophenyl-β-D-xylopyranoside) than arabinosidase activity (determined with substrate 4NPA, 4-nitrophenyl-α-L-arabinofuranoside) and others have the opposite imbalance [8–15], owes to similarity of the glycone residues in three dimensional space such that glycosidic bonds and hydroxyl groups of β-D-xylose and α-L-arabinofuranose glycosides can be overlaid to occupy similar positions [8,11]. XA enzymes have potential utility in industrial processes where they could serve double duty in depolymerizing complex carbohydrates (i.e., arabinoxylans) of herbaceous biomass to simple sugars for subsequent fermentation to fuel ethanol or other bioproducts [16–19]. In this regard, XA from *Selenomonas ruminantium* (SXA) of glycoside hydrolase family 43 (GH43) holds particular interest because it has been

* Corresponding author. Tel.: +1 309 681 6472; fax: +1 309 681 6472.
E-mail address: douglas.jordan@ars.usda.gov (D.B. Jordan).

1570-9639/$ - see front matter. Published by Elsevier B.V.
doi:10.1016/j.bbapap.2007.06.010

revealed as a highly efficient catalyst for promoting hydrolysis of xylooligosaccharides [10,20].

Members of GH43, GH32, GH62, and GH68 possess 5-bladed β propeller domains. X-ray structures have been determined for GH43 XA enzymes isolated from *Bacillus subtilis*, *Bacillus halodurans*, *Clostridium acetobutylicum,* and *Geobacillus stearothermophilus*, which have 53–70% protein sequence identity with SXA [10,21]. The structures manifest a funnel-shaped active site that comprises two subsites with a single route for access by ligands. Structures of catalytically impaired mutant XAs from *G. stearothermophilus* in complex with xylobiose are most useful for modeling ligands in the active site, particularly since there is little change in the positions of amino acid residues of subsite −1 in comparison to the structure of the unliganded wild-type XA [21] and the eight amino acid residues in the vicinity of the xylose moiety of the nonreducing end of xylobiose, which occupy subsite −1, are fully conserved among some GH43 XA enzymes, including SXA and the XA enzymes from *B. subtilis*, *B. halodurans*, *C. acetobutylicum,* and *B. pumilus*. Substrates 4NPX and 4NPA, docked in subsite −1 are shown in Fig. 1. Notably, a hydrogen bonding network is formed among D14, D127, E186, H248, and R290 side chains; the salt bridge between D14 and R290 serves to lower the pK_a of the carboxylate group of D14, the catalytic base; and the pK_a of the carboxylate group of E186, the catalytic acid, is raised by its proximity to D127 [10,21]. Three hydroxyl groups of xylose share H bonds with side chains of D127 and H248 (O2), D127 (O3), and D14 and R290 (O4). Because similar positions are occupied by the O2, O3, and O5 of 4NPA, similar H bonds are shared. Interactions with C2 hydroxyl groups are considered most important to catalysis in GH-mediated reactions [11,22,23].

Biochemical evidence is in accord with structural inferences that SXA (and other GH43 XA enzymes) catalyzes hydrolysis of substrates with inversion of anomeric stereochemistry, implicating a single transition state with the catalytic base (D14) serving to activate a water molecule for addition to substrate and the catalytic acid (E186) serving to protonate the leaving group; SXA catalyzes the hydrolysis of a single residue from the nonreducing end of substrate without processivity so that all products of the hydrolysis reaction are removed from the active site before initiating another catalytic cycle; mutation D127A causes the greatest erosion of catalysis among active-site residues studied;

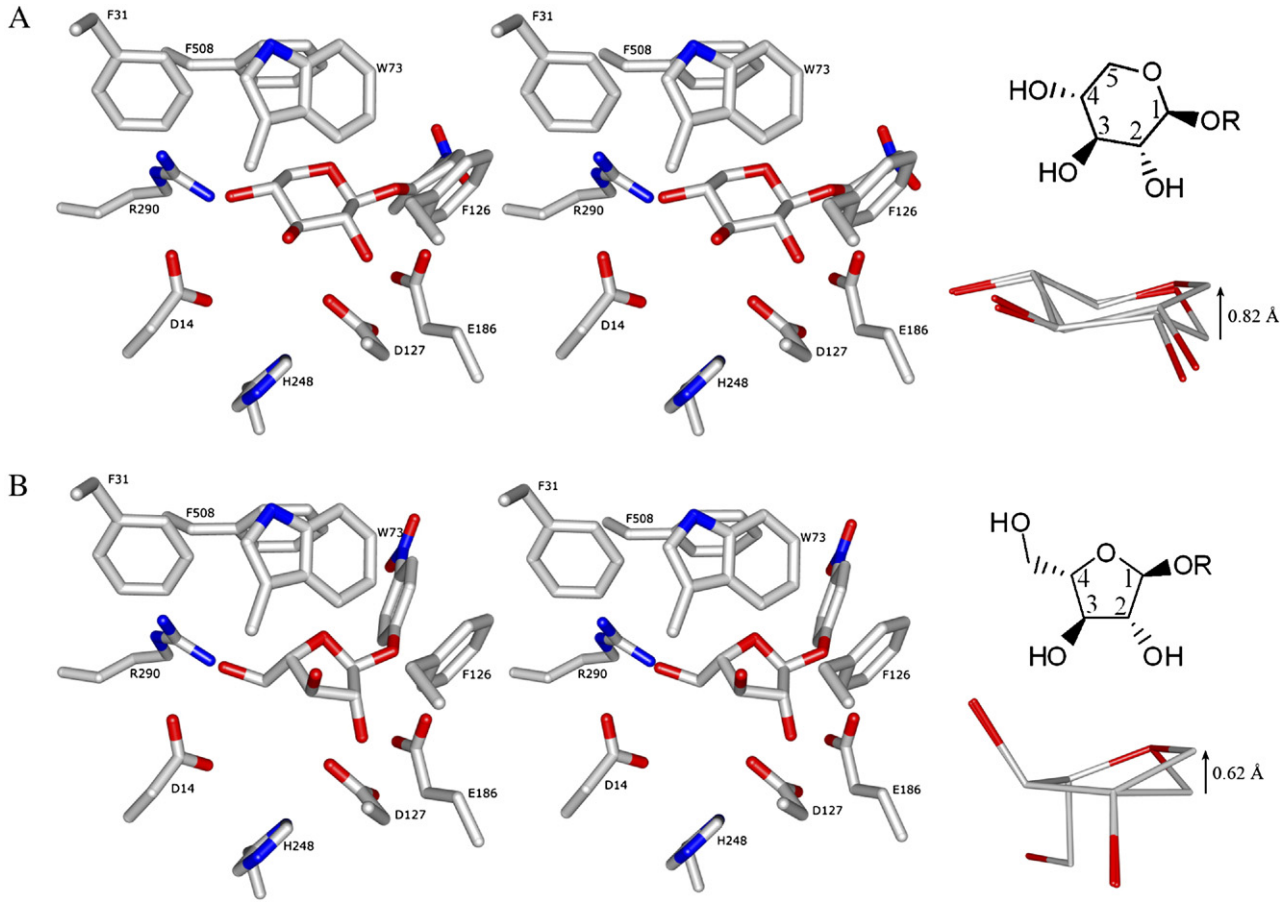

Fig. 1. Stereoview models of the SXA active site (subsite −1) with docked substrates 4NPX and 4NPA. Xylobiose coordinates were transferred from the X-ray structure of catalytically-impaired XA mutant (E186G) from *G. stearothermophilus* (PDB Code 2EXK) to the wild-type XA structure (PDB Code 2EXH). The eight protein residues shown (SXA numbering of residues) are fully conserved in SXA and some other GH43 XA enzymes. 4NPX and 4NPA were docked into the active site by using xylobiose as a guide. (A) 4NPX. Shown to the right: numbering system of xylose ring and distortion of xylose ring so that C1, C2, C5 and O5 are coplanar. (B) 4NPA. Shown to the right: numbering system of arabinofuranose ring and distortion of arabinofuranose ring so that C1, C2, C4 and O4 are coplanar.

and the β-xylosidase and α-arabinofuranosidase activities share the single active site of the SXA protomer [10].

The latter point was addressed with evidence from studies of catalytically impaired mutants of SXA which showed that individual mutations of the catalytic base and catalytic acid to alanine effected erosion of several thousand fold in $(k_{cat}/K_m)^{4NPX}$ and $(k_{cat}/K_m)^{4NPA}$, but relative substrate specificities $(k_{cat}/K_m)^{4NPX}/(k_{cat}/K_m)^{4NPA}$ of D14A and E186A mutations remained similar to wild-type enzyme [10]. The same study exposed that, whereas K_m^{4NPX} values were similar to wild-type SXA for D14A, D127A, H248A, and E186 mutations, the R290A mutation affected a 64-fold increase in K_m^{4NPX}, suggesting that R290 serves as a recognition element for the substrate. It has been noted that, depending on its orientation, the C5 hydroxyl group of 4NPA has potential to conflict with the side-chains of D14, F31, and R290 [21].

In this work we set out to search for which residues, if any, of subsite −1 and in proximity to the glycone, favor the β-xylosidase reaction over the α-arabinofuranosidase reaction. Off the enzyme, hydrolysis of 4NPA occurs more rapidly than 4NPX (the $\Delta\Delta G$ amounts to ~1.6 kcal/mol for 4NPA versus 4NPX at pH 5.3 and 25 °C; D. B. Jordan, unpublished) and this is attributable, in part, to the greater difficulty of the all-equatorial substituted β-D-xylosyl residue of 4NPX than the α-L-arabinosyl residue of 4NPA in achieving geometrical distortion to the transition state [[11,24] and references therein]. SXA-catalyzed reactions have relative substrate specificities $(k_{cat}/K_m)^{4NPX}/(k_{cat}/K_m)^{4NPA}$ of 12.3 and $k_{cat}^{4NPX}/k_{cat}^{4NPA}$ of 11.6 ($\Delta\Delta G$ ~1.5 kcal/mol) [10]. Altogether, there is ~3 kcal/mol window available to dissect for contributions to catalysis that favor 4NPX over 4NPA.

2. Materials and methods

2.1. Materials and general methods

4NPA, 4NPX, and buffers were obtained from Sigma-Aldrich. Water was purified through a Milli-Q unit (Millipore). All other reagents were reagent grade and high purity. A Cary 50 Bio UV-Visible spectrophotometer (Varian), equipped with a thermostatted holder for cuvettes, was used for absorbance spectra and kinetic determinations. An AVIV Model 215 circular dichroism spectrophotometer (Aviv Biomedical), equipped with thermostatted cuvette holder, and a 1-mM path length quartz cuvette were used for acquiring protein spectra; 3–5 spectra were averaged for each protein sample. SXA was cloned from *S. ruminantium*, and expressed in *Escherichia coli* [25]. D14A, D127A, E186A, H248A, and R290A mutants of SXA were prepared and purified to homogeneity in the same manner as wild-type SXA [10]. Manipulations of coordinates (overlays, distance measurements, etc.) were through Swiss-PDB Viewer 3.7 (http://www.expasy.org/spdbv/) [26]. Molecular graphics images were produced using the UCSF Chimera package from the Resource of Biocomputing, Visualization, and Informatics at the University of California, San Francisco (supported by NIH P41 RR-01081) [27].

2.2. Preparation of mutant enzymes

Site-directed mutagenesis was performed using the QuikChange site-directed mutagenesis kit (Stratagene) according to the manufacturer's instructions. Oligonucleotide primers are listed in Table 1. The template was pSRA1 with the SXA gene cloned into pET21(+) [25]. Complete sequences were determined on a Model 3700 sequencer (Applied Biosystems) using T7 promoter and specific primers to confirm that only the intended mutations had been introduced. pSRA1 and its mutated plasmids were used for transformation of *E. coli* BL21(DE3). BL21(DE3) cells containing SXA and SXA mutants were grown and the proteins were purified to homogeneity (judged by SDS-PAGE analysis) as described [10], with the addition of a final desalting, gel filtration step employing a 2.6×30 cm column of Bio-Gel P-6 DG desalting gel (Bio-Rad), equilibrated and developed with 20 mM sodium phosphate, pH 7.0. Mutant proteins behaved similarly to wild-type SXA in terms of high yields in *E. coli* (~30% of soluble protein) and elution times from chromatography columns. Circular dichroism spectra (190–260 nm, collected for samples containing 8 μM enzyme in 18 mM sodium phosphate, 4 mM Tris–HCl, pH 7.3) are characterized by a major trough at 214 nm (reflecting dominance of β structure), and the spectra are similar for wild-type SXA and mutants: mean trough values [[θ]] at 214 nm for three wild-type SXA samples $=(-3.00\pm0.13)\times10^6$ deg·cm^2·dmol^{-1}; mean trough values ([θ]) at 214 nm for the 13 mutant proteins $=(-2.83\pm0.14)\times10^6$ deg·cm^2·dmol^{-1} with a range of $(-2.52$ to $-3.00)\times10^6$ deg·cm^2·dmol^{-1}.

Table 1
Primers used for site-directed mutagenesis of SXA[a]

Mutation	Primer sequence (5′→3′)
F31A	CTATATTGCCACCTCCACCGCCGAGTGGTTCCCCGGTG
	CACCGGGGAACCACTCGGCGGTGGAGGTGGCAATATAG
R290H	CTGTCCGCTGGGCCACGAAACCGCCATCCAAA
	TTTGGATGGCGGTTTCGTGGCCCAGCGGACAG
R290K	CTGTCCGCTGGGCAAGGAAACCGCCATCCAAA
	TTTGGATGGCGGTTTCCTTGCCCAGCGGACAG
R290Q	CTGTCCGCTGGGCCAGGAAACCGCCATCCAAA
	TTTGGATGGCGGTTTCCTGGCCCAGCGGACAG
R290G	CTGTCCGCTGGGCGGAGAAACCGCCATCCAAA
	TTTGGATGGCGGTTTCTCCGCCCAGCGGACAG
R290V	TGTCCGCTGGGCGTCGAAACCGCCATCCA
	TGGATGGCGGTTTCGACGCCCAGCGGACA
W73A	GATTCCGGCGGCATCGCAGCACCTGACCTTTCC
	GGAAAGGTCAGGTGCTGCGATGCCGCCGGAATC
F508A	GCGCGGCGGCGGATTCGCCACTGGTGCTTTCG
	CGAAAGCACCAGTGGCGAATCCGCCGCCGCGC

[a] Underlined nucleotides indicate mutations incorporated into primers.

2.3. Determination of steady-state kinetic parameters

Method A (discontinuous monitoring of reaction progress) was used throughout this work for determination of initial rates. Reactions (20–40 min) were initiated by adding a small aliquot of enzyme (generally 7 μl of enzyme diluted into 10 mM sodium phosphate, pH 7.0, and incubated on wet ice or at ~25 °C) to 1-ml, temperature-equilibrated (25 °C) reaction mixtures containing 100 mM sodium succinate, pH 5.3, and varied concentrations (0.2–7 mM) of 4NPA or 4NPX. Aliquots (0.02–0.2 ml) were removed from reactions at 4- to 6-min intervals, placed into cuvettes containing 0.80–0.98 ml 0.1 M NaOH for 4NPX reactions (or 1 M Na_2CO_3 at pH 11 for 4NPA reactions) so that the final cuvette volume was 1 ml, and the absorbance was read at 400 nm. Initial rates were calculated from fitting the absorbance readings versus time to a line (minimum of 4 points per reaction progression) and absorbencies were converted to molarities by using an extinction coefficient of 18.3 mM^{-1} cm^{-1} for the absorbance of 4-nitrophenol in NaOH [28]. Concentrations of 4NPA and 4NPX were determined by incubating substrate with excess enzyme until an end point was reached, adding an aliquot (0.01 to 0.1 ml) to 0.1 M NaOH, recording the absorbance at 400 nm and using the extinction coefficient of 18.3 cm^{-1} mM^{-1}. The parameter, k_{cat}, is expressed in moles of substrate hydrolyzed per second per mole of enzyme active sites (monomers), the latter calculated from the 280-nm extinction coefficient of 129,600 M^{-1} cm^{-1} for SXA protomers [10,29].

2.4. Equations

Data were fitted to equations using the computer program Grafit (Erithacus Software) [30]. For Eq. (1), v is the observed initial (steady-state) rate of catalysis, k_{cat} is the maximum rate of catalysis, S is the substrate concentration, and K_m is the Michaelis constant. For Eqs. (2)–(4), p is the determined

parameter at a single pH, P is the pH-independent value of the parameter, K_a is the acid dissociation constant of the group affecting P, H^+ is the proton concentration, K_{a1} is the acid dissociation constant of the first group affecting P, K_{a2} is the acid dissociation constant of the second group affecting P, P_1 is the limit of p associated with K_{a1}, and P_2 is the limit of p associated with K_{a2}.

$$v = \frac{k^*_{cat} S}{k_m + S} \quad (1)$$

$$P = \frac{P}{1 + \frac{H^+}{K_{a1}} + \frac{K_{a2}}{H^+}} \quad (2)$$

$$P = \frac{P}{1 + \frac{H^+}{K_a}} \quad (3)$$

$$P = \frac{P_1}{1 + \frac{H^+}{K_{a1}}} + \frac{P_2 - P_1}{1 + \frac{H^+}{K_{a2}}} \quad (4)$$

3. Results and discussion

Steady-state kinetic parameters were determined at pH 5.3 to avoid nonproductive binding of 4NPX to SXA known to occur with the native SXA at higher pH (pK_a 7); such nonproductive binding does not occur with 4NPA [10]. This precaution is unnecessary for comparing relative substrate specificities $(k_{cat}/K_m)^{4NPX}/(k_{cat}/K_m)^{4NPA}$ because k_{cat}/K_m is not affected by nonproductive binding. $(k_{cat}/K_m)^{4NPX}/(k_{cat}/K_m)^{4NPA}$ is nearly pH independent in the pH range 4.3–7 and above pH 7 drops by 25% to a new limit (Fig. 2). The small pH dependence of the relative parameter owes to the similar bell-shaped curves for the individual parameters $(k_{cat}/K_m)^{4NPX}$ (pK_a's 5.03 and 7.21) and $(k_{cat}/K_m)^{4NPA}$ (pK_a's 5.01 and 7.34). However, the pH profiles for parameters k_{cat} and $1/K_m$ differ for the two substrates: the pH dependence of k_{cat}^{4NPX} describes a bell-shaped curve with an acidic limb (pK_a 3.34) and basic limb (pK_a 6.98) and the pH dependence k_{cat}^{4NPA} has only the acidic limb (pK_a 3.49); the pH curve of $(1/K_m)^{4NPX}$ has two acidic limbs (pK_a's 4.95 and 6.71), and that of $(1/K_m)^{4NPA}$ is bell-shaped (pK_a's 4.92 and 7.37). Thus, the relative parameters $k_{cat}^{4NPX}/k_{cat}^{4NPA}$ and $(1/K_m)^{4NPX}/(1/K_m)^{4NPA}$ drop in value at higher pH (pK_a ~7) to endpoints of zero. Similar to the pH profile for $(1/K_m)^{4NPX}$, the $1/K_i$ pH profiles for inhibition of SXA-catalyzed hydrolysis of 4NPX by D-glucose, D-xylose, and L-arabinose exhibit two acidic limbs with pK_a's 5 and 7 [31]. The latter, the determination that kinetic parameters of SXA acting on 4NPX and 4NPA are weakly influenced by the viscosity of reaction mixtures [10], and that some catalytically-impaired mutants exhibit similar K_m values for 4NPX and 4NPA as wild-type SXA [10] suggest that K_m terms reflect binding constants for the substrates. From stopped-flow studies, SXA-catalyzed hydrolysis of 4NPX and 4NPA exhibit neither bursts nor lags, suggesting that the k_{cat} terms reflect the bond-breaking step of catalysis. Therefore, in addition to k_{cat}/K_m values, values for k_{cat} and K_m are presented and discussed for the site-directed mutants of SXA.

Among the eight native residues mutated to alanine, $(k_{cat}/K_m)^{4NPX}/(k_{cat}/K_m)^{4NPA}$ values are similar (values range from 8.52 to 13.0) to the wild-type value of 12.3 for five mutations

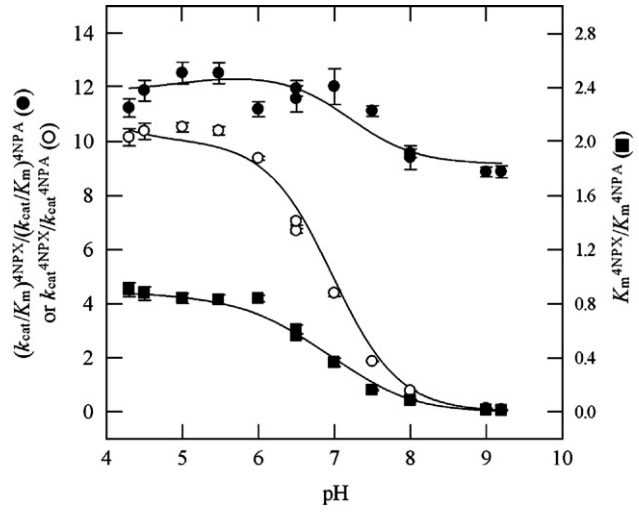

Fig. 2. pH dependencies of relative steady-state kinetic parameters for 4NPX and 4NPA. Kinetic parameters for each substrate were determined at the indicated pH values [10], and pH dependencies of each kinetic parameter were determined by fitting the kinetic parameters (using only those determined when 4NPX and 4NPA reactions contained the same buffer at each pH) to the indicated equations. Eq. (2) for $(k_{cat}/K_m)^{4NPX}$: pH-independent value = 58.6 ± 4.7, pK_{a1} = 5.03 ± 0.07, and pK_{a2} = 7.21 ± 0.06. Eq. (2) for $(k_{cat}/K_m)^{4NPA}$: pH-independent value = 4.69 ± 0.33, pK_{a1} = 5.01 ± 0.06, and pK_{a2} = 7.34 ± 0.05. Eq. (2) for k_{cat}^{4NPX}: pH-independent value = 31.4 ± 2.3, pK_{a1} = 3.34 ± 0.76, and pK_{a2} = 6.98 ± 0.05. Eq. (3) for k_{cat}^{4NPA}: pH-independent value = 3.13 ± 0.06 and pK_a = 3.49 ± 0.19. Eq. (4) for $(1/K_m)^{4NPX}$: middle limit = 1.67 ± 0.16, upper limit = 2.95 ± 0.10 pK_{a1} = 4.95 ± 0.06, and pK_{a2} = 6.71 ± 0.22. Eq. (2) for $(1/K_m)^{4NPA}$: pH-independent value = 1.41 ± 0.14, pK_{a1} = 4.92 ± 0.09, and pK_{a2} = 7.37 ± 0.07. The determined pK_a value(s) and the pH-independent value(s) for each substrate were substituted for the parameters in the respective equations to calculate the values of the parameter between pH 4.3 and 9.2, and the ratio of the respective parameters for 4NPX and 4NPA were calculated and plotted as continuous curves. Actual relative values (±standard errors) are plotted with the indicated symbols. Note that the right ordinate scale is expanded 5-fold in comparison to the left ordinate scale.

(D14A, W73A, D127A, E186A, and H248A), though the individual parameters $(k_{cat}/K_m)^{4NPX}$ and $(k_{cat}/K_m)^{4NPA}$ decline by greater than 99.7% in each case (Table 2). Major erosion (>99.7%) is effected in the k_{cat}^{4NPX} and k_{cat}^{4NPA} terms by D14A, D127A, and E186A mutations, as $(1/K_m)^{4NPX}$ and $(1/K_m)^{4NPA}$ remain within 45% those of wild-type SXA values. For W73A, estimated values for K_m^{4NPA} and K_m^{4NPX} were far greater than the highest substrate concentrations used (solubility limitation of 4NPX and 4NPA; non-saturation kinetics) and consequently, K_m and k_{cat} values cannot be well determined; k_{cat}/K_m values are well determined, however. For H248A, K_m^{4NPX} is increased by 37% and k_{cat}^{4NPX} is eroded by 99.7%; K_m^{4NPA} and k_{cat}^{4NPA} cannot be determined owing to the high value for K_m^{4NPA}. Weak binding of substrates to W73A can be reconciled from its role implicated from the X-ray structures, in forming a pocket to guide substrates to bind in the proximity of residues more directly involved in catalysis. Differential effects on binding of 4NPA and 4NPX conferred by H248A, where H248 is a central residue in the H bonding network comprising D14, D127, E186, H248, and R290, may stem from the noted propensity of 4NPX (xylose with all equatorial OH groups) to find nonproductive binding modes that do not occur with 4NPA [10].

Table 2
Kinetic parameters for wild-type and mutated SXA with substrates 4NPX and 4NPA at pH 5.3 and 25 °C[a]

SXA	k_{cat} (4NPA) (s^{-1})	K_m (4NPA) (mM)	k_{cat}/K_m (4NPA) (s^{-1} mM^{-1})	k_{cat} (4NPX) (s^{-1})	K_m (4NPX) (mM)	k_{cat}/K_m (4NPX) (s^{-1} mM^{-1})	$\frac{k_{cat}/K_m(4NPX)}{k_{cat}/K_m(4NPA)}$
Wild-type[b]	2.68±0.06	0.810±0.050	3.30±0.14	31.1±0.4	0.764±0.031	40.7±1.2	12.3±0.6
D14A[b]	$(9.36\pm0.12)\times10^{-4}$	0.771±0.028	$(1.21\pm0.03)\times10^{-3}$	$(9.56\pm0.16)\times10^{-3}$	0.781±0.035	0.0123±0.0004	10.1±0.4
F31A	9.33±0.65	26.8±2.2	0.348±0.004	0.196±0.002	1.39±0.033	0.142±0.002	0.407±0.008
W73A	ND[c]	ND	$(1.14\pm0.05)\times10^{-3}$	ND	ND	0.0147±0.0008	13.0±0.9
D127A[d]	$(1.34\pm0.08)\times10^{-5}$	0.779±0.136	$(1.72\pm0.22)\times10^{-5}$	$(1.29\pm0.03)\times10^{-4}$	0.881±0.059	$(1.47\pm0.07)\times10^{-4}$	8.52±1.16
E186A[b]	$(2.39\pm0.08)\times10^{-4}$	1.33±0.11	$(1.80\pm0.10)\times10^{-4}$	$(2.67\pm0.05)\times10^{-3}$	1.10±0.05	$(2.42\pm0.08)\times10^{-3}$	13.4±0.9
H248A[d]	ND	ND	$(9.88\pm1.66)\times10^{-3}$	0.0950±0.0025	1.05±0.07	0.0909±0.0044	9.19±1.61
R290A[d]	0.0149±0.0013	7.97±1.01	$(1.87\pm0.08)\times10^{-3}$	0.0126±0.0020	50.3±8.9	$(2.50\pm0.04)\times10^{-4}$	0.134±0.006
R290V	0.0175±0.0005	9.07±0.42	$(1.93\pm0.03)\times10^{-3}$	0.0175±0.0015	33.1±3.2	$(5.30\pm0.06)\times10^{-4}$	0.274±0.006
R290G	$(5.53\pm0.12)\times10^{-3}$	5.10±0.21	$(1.09\pm0.02)\times10^{-3}$	$(3.35\pm0.17)\times10^{-3}$	2.93±0.34	$(1.14\pm0.08)\times10^{-3}$	1.05±0.08
R290H	0.158±0.011	52.1±3.9	$(3.03\pm0.02)\times10^{-3}$	0.0721±0.0020	12.6±0.5	$(5.73\pm0.07)\times10^{-3}$	1.89±0.03
R290K	0.426±0.041	40.5±4.4	0.0105±0.0002	0.325±0.008	7.82±0.28	0.0415±0.0005	3.95±0.08
R290Q	0.275±0.017	17.7±1.4	0.0155±0.003	0.483±0.028	18.1±1.3	0.0267±0.0004	1.72±0.04
F508A	1.09±0.024	5.82±0.23	0.186±0.003	11.4±0.4	13.6±0.6	0.842±0.009	4.51±0.10

[a] Initial-rate data, acquired by using method A, were fitted to Eq. (1) for determination of kinetic parameters. Standard errors (±) are indicated.
[b] 4NPX and 4NPA data from ref. [10].
[c] Not determined because the K_m value is much larger than the largest concentration of substrate (non-saturation kinetics).
[d] 4NPX data from ref [10].

$(k_{cat}/K_m)^{4NPX}/(k_{cat}/K_m)^{4NPA}$ declined from 12.3 for wild-type SXA to 0.407, 0.134 and 4.51 for F31A, R290A, and F508A, respectively (Table 2). The 96.7% decline in the relative parameter of F31A is accompanied by erosion in the individual parameters: $(k_{cat}/K_m)^{4NPX}$ (99.7%), k_{cat}^{4NPX} (99.4%), $(1/K_m)^{4NPX}$ (45.0%), $(k_{cat}/K_m)^{4NPA}$ (89.5%), and $(1/K_m)^{4NPA}$ (97.0%); k_{cat}^{4NPA} increased by 248%. The reduction of 99.8% in $k_{cat}^{4NPX}/k_{cat}^{4NPA}$ accounts for the drop in the relative specificity value, categorizing F31A as a relative k_{cat} effect on $(k_{cat}/K_m)^{4NPX}/(k_{cat}/K_m)^{4NPA}$. F31 resides above the C4 OH group of 4NPX and above the C5 OH group of 4NPA (Fig. 1).

The factor of 92 drop in $(k_{cat}/K_m)^{4NPX}/(k_{cat}/K_m)^{4NPA}$ imposed by the R290A mutation is accompanied by large losses in the individual parameters $(k_{cat}/K_m)^{4NPX}$ (160000-fold loss), k_{cat}^{4NPX} (2500-fold), $(1/K_m)^{4NPX}$ (66-fold), $(k_{cat}/K_m)^{4NPA}$ (1800-fold), k_{cat}^{4NPA} (180-fold), and $(1/K_m)^{4NPA}$ (10-fold). Similar contributions from drops in $k_{cat}^{4NPX}/k_{cat}^{4NPA}$ (14-fold) and $(1/K_m)^{4NPX}/(1/K_m)^{4NPA}$ (6.7-fold) account for the overall drop in relative substrate specificities, categorizing R290A as a relative k_{cat} and relative K_m effect on $(k_{cat}/K_m)^{4NPX}/(k_{cat}/K_m)^{4NPA}$. R290 shares H bonds with and resides below the C4 OH group of 4NPX and below the C5 OH group of 4NPA (Fig. 1).

The 2.7-fold drop in $(k_{cat}/K_m)^{4NPX}/(k_{cat}/K_m)^{4NPA}$ effected by the F508A mutation is accompanied by relatively small drops in the individual parameters: $(k_{cat}/K_m)^{4NPX}$ (48-fold loss), k_{cat}^{4NPX} (2.7-fold), $(1/K_m)^{4NPX}$ (18-fold), $(k_{cat}/K_m)^{4NPA}$ (18-fold), k_{cat}^{4NPA} (2.5-fold), and $(1/K_m)^{4NPA}$ (7.2-fold). The drop in relative substrate specificity derives predominantly from the drop in $(1/K_m)^{4NPX}/(1/K_m)^{4NPA}$ of 2.5-fold, categorizing the mutation as a relative K_m effect on $(k_{cat}/K_m)^{4NPX}/(k_{cat}/K_m)^{4NPA}$. F508 resides near the C4 and C5 groups of 4NPX and 4NPA, where hydrophobic interactions can occur; hydrophobic interactions with 4NPX are expected to exceed those of 4NPA owing to the C4 methylene of 4NPX. Such interactions between ground state and transition state geometries of substrates and hydrophobic side chains of active-site residues are a common feature of GH enzymes; the side chains have been termed, the "hydrophobic platform" and the interacting portion of the glycone, "the hydrophobic patch" [32].

The R290A mutation affects the greatest change (92-fold drop) in $(k_{cat}/K_m)^{4NPX}/(k_{cat}/K_m)^{4NPA}$. This mutation was followed up with mutation of R290 to additional residues resulting in the following declines in $(k_{cat}/K_m)^{4NPX}/(k_{cat}/K_m)^{4NPA}$: R290V (45-fold), R290G (12-fold), R290Q (7.2-fold), R290H (6.5-fold), and R290K (3.1-fold). Thus, the $(k_{cat}/K_m)^{4NPX}/(k_{cat}/K_m)^{4NPA}$ values for position 290 decline from wild-type in the order R>K>H>Q>G>V>A. The progression of relative substrate specificity values approximates the physiochemical similarities of the residues to R and resembles the progression for similarity to R obtained from a Point Accepted Mutation matrix (PAM250): R>K>H>Q>V=A>G [33]. Thus, it can be inferred that mutation of R290 is specific, maintaining an organized active site. Individual parameters have the progressions: k_{cat}/K_m^{4NPX} (wild-type R290>K>Q>H>G>V>A), k_{cat}^{4NPX} (wild-type R290>Q>K>H>V>A>G), $1/K_m^{4NPX}$ (wild-type R290>G>K>H>Q>V>A), k_{cat}/K_m^{4NPA} (wild-type R290>Q>K>H> V>A>G), k_{cat}^{4NPA} (wild-type R290>K>Q>H>V>A>G), and $1/K_m^{4NPA}$ (wild-type R290>G>A>V>Q>K>H). Relative parameters have the progressions: $k_{cat}^{4NPX}/k_{cat}^{4NPA}$ (wild-type R290>Q>V>A>K>G>H) and $1/K_m^{4NPX}/1/K_m^{4NPA}$ (K>H>G>wild-type R290>Q>V>A). Taken together, relative substrate specificities of R290 mutations are perturbed by combinations of relative effects on k_{cat} and K_m.

Among the 8 subsite −1 residues interrogated for their contribution to catalysis by trimming their side chains to the methyl group of alanine, severity of loss in individual substrate specificity values follows the progressions: for $(k_{cat}/K_m)^{4NPX}$, D127>R290>E186>D14>W73>H248>F31>F508, and for $(k_{cat}/K_m)^{4NPA}$, D127>E186>W73A>D14>R290>H248>F508>F31. At the top of both progressions is D127 and in the top half of both progressions are E186 and D14. Thus, the native residues are highly important to catalyzing hydrolysis of both 4NPX and 4NPA: D127, for its role in H bonding with O2 and O3

of substrate and D14 and E186, for roles as catalytic base and catalytic acid. Their mutation to alanine has little effect on the relative substrate specificity. Changes in relative substrate specificities are conferred by R290A, which is among the top half of residues whose change adversely affects $(k_{cat}/K_m)^{4NPX}$ and in the bottom half of residues whose change adversely affects $(k_{cat}/K_m)^{4NPA}$, and by F31A and F508A, which reside in the bottom half of residue changes that negatively affect $(k_{cat}/K_m)^{4NPX}$ and $(k_{cat}/K_m)^{4NPA}$. This underscores that determinants of $(k_{cat}/K_m)^{4NPX}/(k_{cat}/K_m)^{4NPA}$ are not necessarily the most important residues for maximizing individual kinetic parameters. F31, R290, and F508 represent three distinct categories of positive contributions to $(k_{cat}/K_m)^{4NPX}/(k_{cat}/K_m)^{4NPA}$ of wild-type SXA: F31, relative k_{cat} effect; R290, relative k_{cat} and relative $1/K_m$ effects; and F508, relative $1/K_m$ effect. Since F508 has little influence on $k_{cat}^{4NPX}/k_{cat}^{4NPA}$ (F508A value = 12.5; wild-type SXA = 11.6), the role of F508 is in substrate recognition that favors 4NPX over 4NPA, whereas F31 and R290 residues contribute higher ratios of $k_{cat}^{4NPX}/k_{cat}^{4NPA}$ and provide differential control of 4NPX and 4NPA reactions apart from substrate binding events.

In achieving the transition-state geometry required by stereoelectronic theory, 4NPX must attain coplanarity of C1, C2, C5 and O5 in the xylose ring and 4NPA, coplanarity of C1, C2, C4 and O4 in the arabinofuranose ring. Such changes from the ground-state geometries can be met, for the most part, by raising C1 of 4NPA and 4NPX while maintaining nearly static positions of the remaining ring atoms (Fig. 1). Movement of C1 is well documented by X-ray studies of retaining GH enzymes that compare structures of Michaelis complexes with structures of trapped covalent intermediate complexes that are linked between the catalytic nucleophile and glycone C1 [11,34,35]. In the models we propose for SXA-catalyzed hydrolysis of 4NPX and 4NPA, R290 and F31 serve to stabilize the position of C4 of the 4NPX glycone (through interactions with O4) and the 4NPA glycone (through interactions with O5) so that the position of C1 can be raised for distorting the glycone rings to achieve the necessary coplanar positions. Thus, R290 and F31 could serve as anchors at the opposite end of the glycones from C1, so that as C1 migrates to its transition-state position, work is focused on distorting ring geometry rather than dispersed by raising the entire ring system or tilting the glycone (as in a seesaw). Requirements for greater movement of C1 and greater energy of ring distortion by β-D-xylopyranose than α-L-arabinofuranose account for the more severe affects of R290A and F31A mutations on 4NPX reactions than 4NPA reactions. Upon binding substrate xylobiose, subsite −1 residues change positions very little from the unliganded state [21]; thus, SXA can be considered preformed to favor more reactive conformations of substrate, termed near attack conformations or NACs [36]. The proposed mechanism for ring distortion in the SXA reactions resembles the proposed mechanism in the pre-organized active site of scytalone dehydratase where one end of the bicyclic substrate is anchored by H bonds between an N residue and substrate's phenolic OH group as the opposite end of substrate is pushed downward by a highly mobile F residue and pulled downward by H bonds between substrate's C3 OH group and a H residue [37]. The scytalone dehydratase mechanism of substrate distortion was brought to light by comparing relative substrate specificities for substrates that differ in energies needed for ring distortion (to transition-state geometries mandated by stereoelectronic principles) harbored by site-directed mutants and wild-type enzyme. By employing a similar strategy for SXA, we believe anchoring residues of SXA (F31 and R290) have been identified; missing is identification of enzyme residue (s) of subsite +1, if any, that favor C1 migration (the force).

Acknowledgments

We thank Jay D Braker and Jennifer Hansen for excellent technical assistance in contributing to this work. This work was supported by USDA funding of CRIS 3620-41000-118. The mention of firm names or trade products does not imply that they are endorsed or recommended by the US Department of Agriculture over other firms or similar products not mentioned.

References

[1] B. Henrissat, A classification of glycosyl hydrolases based on amino acid sequence similarities, Biochem. J. 280 (1991) 309–316.
[2] B. Henrissat, G.J. Davies, Structural and sequence-based classification of glycoside hydrolases, Curr. Opin. Struct. Biol. 7 (1997) 637–644.
[3] B. Henrissat, Glycosidase families, Biochem. Soc. Trans. 26 (1998) 153–156.
[4] V.L. Yip, S.G. Withers, Nature's many mechanisms for the degradation of oligosaccharides, Org. Biomol. Chem. 2 (2004) 2707–2713.
[5] A. Vasella, G.J. Davies, M. Böhm, Glycosidase mechanisms, Curr. Opin. Chem. Biol. 6 (2002) 619–629.
[6] D.L. Zechel, S.G. Withers, Glycosidase mechanisms: anatomy of a finely tuned catalyst, Acc. Chem. Res. 33 (2000) 11–18.
[7] M.L. Sinnott, Catalytic mechanism of enzymic glycosyl transfer, Chem. Rev. 90 (1990) 1171–1202.
[8] R.C. Lee, M. Hrmova, R.A. Burton, J. Lahnstein, G.B. Fincher, Bifunctional family 3 glycoside hydrolases from barley with (α-L-arabinofuranosidase and (β-D-xylosidase activity. Characterization, primary structures, and COOH-terminal processing, J. Biol. Chem. 278 (2003) 5377–5387.
[9] Z. Minic, C. Rihouey, C.T. Do, P. Lerouge, L. Jouanin, Purification and characterization of enzymes exhibiting β-D-xylosidase activities in stem tissues of Arabidopsis, Plant Physiol. 135 (2004) 867–878.
[10] D.B. Jordan, X.-L. Li, C.A. Dunlap, T.R. Whitehead, M.A. Cotta, Structure–function relationships of a catalytically efficient β-D-xylosidase, Appl. Biochem. Biotechnol. 141 (2007) 51–76.
[11] K. Hövel, D. Shallom, K. Niefind, V. Belakhov, T. Baasov, Y. Shoham, D. Schomburg, Crystal structure and snapshots along the reaction pathway of a family 51 α-L-arabinofuranosidase, EMBO J. 22 (2003) 4922–4932.
[12] I. Smaali, C. Rémond, M.J. O'Donohue, Expression in *Escherichia coli* and characterization of β-xylosidases GH39 and GH-43 from *Bacillus halodurans* C-125, Appl. Microbiol. Biotechnol. 73 (2006) 582–590.
[13] D. Shallom, M. Leon, T. Bravman, A. Ben-David, G. Zaide, V. Belakhov, G. Shoham, D. Schomburg, T. Baasov, Y. Shoham, Biochemical characterization and identification of the catalytic residues of a family 43 β-D-xylosidase from *Geobacillus stearothermophilus* T-6, Biochemistry 44 (2005) 387–397.
[14] W. Shao, J. Wiegel, Purification and characterization of a thermostable β-xylosidase from *Thermoanaerobacter ethanolicus*, J. Bacteriol. 174 (1992) 5848–5853.
[15] E.A. Utt, C.K. Eddy, K.F. Keshav, L.O. Ingram, Sequencing and expression of the *Butyrivibrio fibrisolvens* xylB gene encoding a novel bifunctional protein with β-D-xylosidase and α-L-arabinofuranosidase activities, Appl. Environ. Microbiol. 57 (1991) 1227–1234.

[16] B.C. Saha, Hemicellulose bioconversion, J. Ind. Microbiol. Biotech. 30 (2003) 279–291.
[17] B.C. Saha, α-L-Arabinofuranosidases: biochemistry, molecular biology and application in biotechnology, Biotechnol. Adv. 18 (2000) 403–423.
[18] K.A. Gray, L. Zhao, M. Emptage, Bioethanol, Curr. Opin. Chem. Biol. 10 (2006) 141–146.
[19] D. Shallom, Y. Shoham, Microbial hemicellulases, Curr. Opin. Microbiol. 6 (2003) 219–228.
[20] D.B. Jordan, X.-L. Li, C.A. Dunlap, T.R. Whitehead, M.A. Cotta, β-D-xylosidase from *Selenomonas ruminantium* of glycoside hydrolase family 43, Appl. Biochem. Biotechnol. 136–140 (2007) 93–104.
[21] C. Brüx, A. Ben-David, D. Shallom-Shezifi, M. Leon, K. Niefind, G. Shoham, Y. Shoham, D. Schomburg, The structure of an inverting GH43 β-xylosidase from *Geobacillus stearothermophilus* with its substrate reveals the role of the three catalytic residues, J. Mol. Biol. 359 (2006) 97–109.
[22] J.D. McCarter, M.J. Adam, S.G. Withers, Binding energy and catalysis. Fluorinated and deoxygenated glycosides as mechanistic probes of *Escherichia coli* (*lac*Z) β-galactosidase, Biochem. J. 286 (1992) 721–727.
[23] M.N. Namchuk, S.G. Withers, Mechanism of Agrobacterium β-glucosidase: kinetic analysis of the role of noncovalent enzyme/substrate interactions, Biochemistry 34 (1995) 16194–16202.
[24] M.L. Sinnott, S.S. Wijesundera, Preparation and conformation of α-L-arabinofuranosyl-pyridinium salts, and hydrolysis of the 4-bromoisoquinolinium compound, Carbohydr. Res. 136 (1985) 357–368.
[25] T.R. Whitehead, M.A. Cotta, Identification of a broad-specificity xylosidase/arabinosidase important for xylooligosaccharide fermentation by the ruminal anaerobe *Selenomonas ruminantium* GA192, Curr. Microbiol. 43 (2001) 293–298.
[26] N. Guex, M.C. Peitsch, SWISS-MODEL and the Swiss-PdbViewer: an environment for comparative protein modeling, Electrophoresis 18 (1997) 2714–2723.
[27] E.F. Pettersen, T.D. Goddard, C.C. Huang, G.S Couch, D.M. Greenblatt, E.C. Meng, T.E. Ferrin, UCSF Chimera — a visualization system for exploratory research and analysis, J. Comput. Chem. 25 (2004) 1605–1612.
[28] F.J. Kezdy, M.L. Bender, The kinetics of the α-chymotrypsin-catalyzed hydrolysis of *p*-nitrophenyl acetate, Biochemistry 1 (1962) 1097–1106.
[29] S.C. Gill, P.H. von Hippel, Calculation of protein extinction coefficients from amino acid sequence data, Anal. Biochem. 182 (1989) 319–326.
[30] R.J. Leatherbarrow, Grafit Version 5, Erithacus Software Ltd., Horley, UK, 2001.
[31] D.B. Jordan, J.D. Braker, Inhibition of the two-subsite β-D-xylosidase from *Selenomonas ruminantium* by sugars: competitive, noncompetitive, double binding, and slow binding modes, Arch. Biochem. Biophys, in press. doi:10.1016/j.abb.2007.05.016.
[32] W. Nerinckx, T. Desmet, M. Claeyssens, A hydrophobic platform as a mechanistically relevant transition state stabilising factor appears to be present in the active centre of all glycoside hydrolases, FEBS Lett. 538 (2003) 1–7.
[33] M.O. Dayhoff, R.M. Schwartz, B.C. Orcutt, A model of evolutionary change in proteins, in: M.O. Dayhoff (Ed.), Atlas of Protein Sequence and Structure, vol. 5, National Biomedical Research Foundation, Washington, 1978, pp. 345–352.
[34] D.J. Vocadlo, G.J. Davies, R. Laine, S.G. Withers, Catalysis by hen egg-white lysozyme proceeds via a covalent intermediate, Nature 412 (2001) 835–838.
[35] A. Varrot, G.J. Davies, Direct experimental observation of the hydrogen-bonding network of a glycosidase along its reaction coordinate revealed by atomic resolution analyses of endoglucanase Cel5A, Acta Crystallogr., D Biol. Crystallogr. 59 (2003) 447–452.
[36] T.C. Bruice, S.J. Benkovic, Chemical basis for enzyme catalysis, Biochemistry 39 (2000) 6267–6274.
[37] Y.-J. Zheng, G.S. Basarab, D.B. Jordan, Roles of substrate distortion and intramolecular hydrogen bonding in enzymatic catalysis by scytalone dehydratase, Biochemistry 41 (2002) 820–826.